

AB-INITIO STUDY OF STRUCTURE AND DYNAMICAL PROPERTIES OF CRYSTALLINE ICE

W. A. ADEAGBO*, A. ZAYAK and P. ENTEL

Institute of Physics,

University of Duisburg-Essen, Duisburg campus, 47048 Duisburg, Germany

(Received March 23, 2022)

Abstract

We investigated the structural and dynamical properties of a tetrahedrally coordinated crystalline ice from first principles based on density functional theory within the generalized gradient approximation with the projected augmented wave method. First, we report the structural behaviour of ice at finite temperatures based on the analysis of radial distribution functions obtained by molecular dynamics simulations. The results show how the ordering of the hydrogen bonding breaks down in the tetrahedral network of ice with entropy increase in agreement with the neutron diffraction data. We also calculated the phonon spectra of ice in a $3 \times 1 \times 1$ supercell by using the direct method. So far, due to the direct method used in this calculation, the phonon spectra is obtained without taking into account the effect of polarization arising from dipole-dipole interactions of water molecules which is expected to yield the splitting of longitudinal and transverse optic modes at the Γ -point. The calculated longitudinal acoustic velocities from the initial slopes of the acoustic mode is in a reasonable agreement with the neutron scattering data. The analysis of the vibrational density of states shows the existence of a boson peak at low energy of translational region a characteristic common to amorphous systems.

Keywords: Ice, Density functional theory, Molecular dynamics, Lattice dynamics.

*Corresponding author. Tel. +49 203 379 1606; fax: +49 203 379 3665.
E-mail: adeagbo@thp.uni-duisburg.de

1. INTRODUCTION

Ice, the frozen form of liquid water, is one of the most common materials on earth and in outer space, and has important relevance to a large number of diverse fields such as astronomy, geophysics, chemical physics, life sciences, etc. (Petrenko and Whitworth, 1999). Ice-Ih, the hexagonal form of ice is the most commonly known phase of ice in which each oxygen atom has four neighbours at the corners of a tetrahedron. When water freezes the forces of interaction between H_2O molecules win over their thermal motion and they form a most stable arrangement precisely with hexagonal symmetry. This is the reason why snow flake crystals are always hexagonal. The crystal structure of ice at the atomic level marks the way these crystals will look. The hydrogen atoms are covalently bonded to the nearest oxygen atoms to form water molecules which are linked to each other through hydrogen bonds. The high translational symmetry is not retained at the level of the crystallographic unit cell. The phase diagram of ice is very complex with over 12 known phases existing, (see Fig. 1). Besides the environmental importance, ice is also special because of the interesting phenomena contained within its structure. The crystal structure of ice is very unusual because, while the molecules lie on a regular crystal lattice, there is disorder in their orientations. This property leads to many interesting characteristics in electrical polarization and conductivity.

Numerous attempts have been made for the past decades to understand the nature of the lattice vibrations of ice, in particular, ice-Ih (Marchi, Tse and Klein, 1986). Experimental information has been obtained from infrared absorption (Whalley and Bertie, 1967), Raman scattering (Klug and Whalley, 1978) and both coherent and incoherent inelastic neutron scattering (Renker and Blanckenhagen, 1969; Prask and Trevino, 1972). On the theoretical side, three basic approaches have been adopted to study the lattice modes. The earliest studies involved the application of lattice dynamics to hypothetical proton ordered structures (Whalley and Bertie, 1967; Prask and Trevino, 1972). Later lattice dynamics was used to study more realistic orientationally disordered structures (Nielsen, Townsend and Rice, 1984). The most recent work has utilized the molecular dynamics simulation techniques (Tse, Klein and McDonald, 1984). Many of these theoretical studies involved the use of classical modeled potential through empirical method in order to describe the interaction of the system (Marchi, Tse and Klein, 1986; Nielson, Townsend and Rice, 1984). As result of all these works, the overall features of the lattice mode spectrum in the translational region ($0\text{-}300\text{ cm}^{-1}$) and in the librational region ($450\text{-}950\text{ cm}^{-1}$) are reasonably well understood. Potential-based empirical modelling has had some success towards the end, but to date, there are no empirical potentials capable of describing the ice dynamics and related properties across its whole spectra range and describing certain key spectra features.

The ab-initio method has recently gained ground not only because of its relia-

bility in the study of static and dynamics properties of ice (Cote, Morrison, Cui, Jenkins *et al.*, 2003; Morrison and Jenkins, 1999) but also because the method allow to model some important features such as the ordered periodic ice structure (Lee, Vanderbilt, Laarson, 1993), and the nature of hydrogen bond in different geometries (Xantheas and Dunning, 1993). Our present study to understand the microscopic nature and lattice vibrations of ice-Ih makes use of the Vienna *Ab Initio* Simulation Package (VASP) (Kresse and Futhmüller, 1996) which is designed to perform ab-initio quantum-mechanical molecular dynamics using pseudopotentials and a plane wave basis set and the recent implementation of the projected augmented wave (PAW) method.

The computational study presented in this work begins with the choice of unit cell of ice as described in Section 2, which is followed by molecular dynamics simulation of ice in a supercell (Section 3) with the unit cell replicated in all directions in order to obtain the structural behaviour in comparison with the available experimental data. In Section 4 and 4.1 we present the results of calculated phonon spectrum of ice in the translational region, which is done in a $3 \times 1 \times 1$ supercell in y -direction, as well as the corresponding integrated vibrational density of states in Section 4.2. The anomalous behaviour of this ice structure observed in the low energy region is presented in Section 4.3. The final Summary of this work is presented in Section 5.

2. COMPUTATIONAL DETAILS

As mentioned above, the calculations in this work were carried out by using the Vienna *Ab Initio* Simulation Package (VASP) (Kresse and Futhmüller, 1996) which has been designed for ab-initio quantum-mechanical molecular dynamics simulations using pseudopotentials and a plane wave basis set and the recent implementation of projected augmented wave (PAW) method. In order to investigate the structural properties of ice, we started with the construction of ice crystal using the Bernal and Fowler rule (Bernal and Fowler, 1933). The rule is based on a statistical model of the position of hydrogen atoms produced by Pauling (Pauling, 1935) using the six possible configurations of hydrogen atoms within Ice Ih. It is defined as ideal crystal based on the assumptions that:

- Each oxygen atom is bonded to two hydrogen atoms at a distance of 0.95 Å to form a water molecule;
- Each molecule is oriented so that its two hydrogen atoms face two, of the four, neighbouring oxygen atoms in the tetrahedral coordination;
- The orientation of adjacent molecules is such that only one hydrogen atom lies between each pair of oxygen atoms;

- Ice Ih can exist in any of a large number of configurations, each corresponding to a certain distribution of hydrogen atoms with respect to oxygen atoms.

The schematic drawing shown in Fig. 2 satisfies one out of the six possible orientations of protons of the central water molecule according to these rules. Each of the oxygen atoms can be linked to another oxygen by the combination of a covalent bond plus a hydrogen bond to form the tetrahedral arrangement of oxygen atoms. A unit cell of this ice was prepared in a cubic box according to Fig. 3 with 8 molecules of water. All the atomic degrees of freedom were relaxed using VASP with the projected-augmented wave (PAW) formalism at high precision. The optimum Monkhorst Pack $4 \times 4 \times 4$ k -point was used in addition to the generalized gradient approximation (GGA) of Perdew-Wang in order to describe the exchange-correlation and to give good description of the hydrogen bonding of water. We used a energy cut-off of 500 eV because the 2p valence electrons in oxygen require a large plane wave basis set to span the high energy states described by the wavefunction close to the oxygen nucleus and also the hydrogen atoms require a larger number of planes waves in order to describe localization of their charges in real space. The lattice constants of the unit cell were calculated from the plot of the energy against the volume. The estimated values of the lattice constants are $a = 6.1568 \text{ \AA}$, $b = 6.1565 \text{ \AA}$, $c = 6.0816 \text{ \AA}$. The values of $a \approx b \neq c$ imply that the relaxed structure is tetragonal with c/a ratio ≈ 0.988 . The experimental lattice constant reported by Blackman *et. al.* (Blackman and Lisgarten, 1958) is 6.35012652 \AA for the cubic geometry. The final geometry obtained was used in our molecular and lattice dynamical study of ice.

3. MOLECULAR DYNAMICS

In our molecular dynamics simulation, the final relaxed geometry in Fig. 2 (or Fig. 3) was replicated in all directions using the calculated values of the lattice parameters to produce 64 molecules of water which form the hexagonal structure shown in Fig. 4. Here the molecular dynamics simulation was done for the Γ -point only in a box of dimension $12.411356 \times 12.411356 \times 12.259675 \text{ \AA}^3$ corresponding to the density 1.01 gcm^{-3} to be compared to the real density of ice Ih and ice Ic which is 0.92 gcm^{-3} . Molecular dynamics was carried out for 3 ps using a time step of 0.5 fs. The angle H-O-H of the ice structure was compared with liquid water at the different temperatures as can be seen in Fig. 5. For ice structure, the H-O-H angle was found to be 107.8° compared to liquid water case at different temperature or isolated water molecule also calculated with VASP which is found to be 104.5° and 105.4° degree, respectively, as can be seen in Fig. 5. The angle shown by solid ice is an indication that the oxygen centre preserves its tetrahedral structural units. Also, the range of the angular distribution for the high temperature

water (or supercritical water) is wider and broader than the corresponding liquid water at ambient temperature and the solid ice cases.

The radial distribution functions for the solid ice accumulated over a 3 ps run are plotted at two different temperatures, 100 K and 220 K. The g_{OO} and g_{OH} in Fig. 6, and g_{HH} in Fig. 7 at 100 K, all exhibit the long-range like order when compared to the short range order of liquid water. There is a well pronounced first peak of g_{OO} at 2.75 Å at 100 K and also the position of the first minimum is deeper when compared to the liquid water radial distribution functions. This result is comparable to the result obtained using the classical TIP4P modelled potential (Svishchev and Kusalik, 1994). The result of the radial distribution function of oxygen atoms, g_{OO} , oxygen-hydrogen atoms g_{OH} (Fig. 8), and hydrogen atoms (Fig. 9) at 220 K were fairly comparable with available neutron diffraction scattering data of Soper (Soper, 2000). The position of the first peak (VASP calculation) shows very little difference from 100 K while the height of the peak is lower for 220 K due to the effect of entropy increase of the hydrogen atoms which results from re-orientation of protons that tends to force apart more oxygen atoms to a larger distance. The positions of the second minimum for 100 K and 220 K solid ice are, respectively, 4.8 Å and 4.9 Å. The experimental result is slightly shifted to the right to the value 5.1 Å for 220 K. The deviation from experimental value might be due to the phase of crystalline ice under consideration.

4. LATTICE DYNAMICS

In this study phonon dispersion curves are calculated by using the PHONON package developed by K. Palinski (Parlinski, 2002) which has been designed to take input data of Hellmann-Feymann forces calculated with the help of an *ab-initio* electronic structure simulation program such as VASP. We carried out the lattice dynamics study of ice by using the geometry of eight-molecule primitive cell discussed in the Section 1. The calculations of force constants was carried out by considering a $3 \times 1 \times 1$ supercell containing 24 molecules of water which is obtained by matching 3 tetragonal unit cells. At the first step of the calculation, the PHONON package is used to define the appropriate crystal supercell for use of the direct method. As done for the primitive unit cell, all the internal coordinates were relaxed until the atomic forces were less than 10^{-4} eV/Å. The relaxed geometry for a $1 \times 1 \times 1$ supercell from the initial configurations containing 8 molecules is shown in Fig. 3. The starting geometry of the molecules in the simulation box shown is such that no hydrogen bonds were present but the positions of oxygen atoms follow the tetrahedral orientation. After the relaxation, all the protons perfectly point to the right direction of oxygen atoms and make the required hydrogen bonds necessary as indicated by the dotted lines in Fig. 3 to preserve the tetrahedral orientation of the ice structure.

Figure 10(I) shows the Brillouin zone belonging to the relaxed structure

of our (model) ice shown in Fig. 3. Figure 10(II) shows the Brillouin zone used in the analysis of the measured phonon spectra for the model structure of D₂O ice. Let us say once again that the relaxed structure shown in Fig. 3 has the long-range orientational order while the actual structure of ice Ih has no long-range orientational order. Therefore, in the analysis of the measured phonon dispersion curves of D₂O, one uses another model for ice shown in Fig. 4. We have to keep this in mind when comparing our calculated dispersion curves with the measured frequencies. For the evaluation of the phonon dispersion curves we have used the direct *ab-initio* force constant method (Parlinski, Li and Kawazoe, 1997), whereby the forces are calculated with VASP via the Hellmann-Feymann theorem in the total energy calculations. Usually, the calculations are done for a supercell with periodic boundary conditions. In such a supercell, a displacement $\mathbf{u}(0, k)$ of a single atom induces forces $\mathbf{F}(lk)$ acting on all other atoms,

$$F_{\alpha}(lk) = \sum_{l'k'\beta} \Phi_{\alpha\beta}(lk; l'k') u_{\beta}(l'k'). \quad (1)$$

This expression allows to determine the force constant matrix directly from the calculated forces (see Parlinski *et. al.*) (Parlinski, Li and Kawazoe, 1997; Parlinski, 2002). The phonon dispersion branches calculated by the direct method are exact for discrete wave vectors defined by the equation

$$\exp(2\pi i \mathbf{k}_L \cdot \mathbf{L}) = 1, \quad (2)$$

where $\mathbf{L} = (L_a, L_b, L_c)$ are lattice parameters of the supercell. A related technique has recently been used to obtain accurate full phonon dispersions in highly symmetric structures of Ni₂GaMn (Zayak, Entel, Enkovaara, Ayuela *et al.*, 2003).

In order to obtain the complete information of the values of all force constants, every atom of the primitive unit cells was displaced by 0.02 Å in both positive and negative non-coplanar, x , y and z directions to obtain pure harmonicity of the system. We use a $3 \times 1 \times 1$ supercell which implies that 3 points in the direction [100] are treated exactly according to the direct method. The points are $[\zeta 00]$, with $\zeta = 1, 1/3, 2/3$. We calculate forces induced on all atoms of the supercell when a single atom is displaced from its equilibrium position, to obtain the force constant matrix, and hence the dynamical matrix. This is then followed by diagonalization of the dynamical matrix which leads to a set of eigenvalues for the phonon frequencies and the corresponding normal-mode eigenvectors. The vibrational density of states (VDOS) is obtained by integrating over k -dependent phonon frequencies from the force-constant matrix in supercells derived from the primitive molecule unit cells.

4.1 Phonon dispersions of crystalline ice

The phonon dispersion curves calculated for our ice crystal in $[100]$ direction are shown in Fig. 11 for low lying energy vibrations. According to the geometry of the supercell, the low-frequency (or low-energy 0-50 meV) acoustic modes can be compared to Renker’s inelastic neutron scattering measurement (Renker, 1973) along the $[0001]$ direction (ΓA) of hexagonal symmetry shown in Fig. 10, taken from reference (Li, 1996), though our calculation was done only along the Cartesian direction $[100]$ of the cubic cell. Our transverse and longitudinal acoustic (LA/TA) dispersions are well behaved when compared to some other modelled calculations or experimental results (Renker, 1973) in the high symmetry directions ΓA of hexagonal ice as shown in Fig. 11(c). We can also compare our result to the Cote *et. al.* result in Fig. 11(b) (Cote, Morrison, Cui, Jenkins *et al.*, 2003), where they have recently used the *ab-initio* method to obtain the phonon dispersions in the translational frequency range for the ice structure in the Brillouin zone of the orthorhombic eight-molecule unit cell. Altogether our LA and TA dispersions are better than Cote’s LA/TA in comparison to the experimental curves in Fig. 11(c). Our dispersion curves in $[100]$ direction can as well be compared to the dispersion curves obtained using a dynamical model with two force constants to describe the low frequencies of vibrations of hexagonal ice as proposed by Faure (Faure, 1969).

Although everywhere along the Γ -point, our dispersions are completely degenerate in the optic region whereas Cote’s dispersions in Fig. 11(b) show some splittings, the so-called longitudinal/transversal optic (LO/TO) splittings whose origins is explained below, while at the zone boundary, some of the dispersions are non-degenerate unlike our results. Our inability to reproduce these splittings at the Γ -point is due to the direct method approach in which absolute periodicity of the crystal according to Born-von Kármán conditions was considered. The splitting of LO and TO branches for long wavelengths occurs in almost all crystals which are heteropolar (partially ionic such as GaAs) or ionic (such as NaCl) at the Γ -point, and only for infrared active modes (Srivastava, 1990). The long-range part of the Coulomb interaction causes the splitting of the $k = 0$ optic modes raising the frequency of LO modes above those of TO modes. The long-range part of the Coulomb interaction corresponds to the macroscopic electric field arising from ionic displacements. Ice is a tetrahedrally covalently bonded polar system whose dipole-dipole interactions give rise to the electric field when they are disturbed. The origin of the splitting is therefore the electrostatic field created by long wavelength modes of vibrations in such crystals. Usually a microscopic electric field influences only the LO modes while TO modes remain unaltered. The field therefore breaks the Born-von Kármán conditions, as a consequence with a direct method only finite wave vector $\mathbf{k} \neq 0$ calculations are possible. Elongated sub-supercells are needed to recover the $\mathbf{k} \rightarrow 0$ limit of the LO phonon branch (Parlinskin, 2002).

In our result there are two transverse acoustic branches which are highly degenerate and a longitudinal acoustic branch. The first optical branch of the dispersion curves is degenerate with the transverse acoustic branches at energy ~ 9.0 meV. The transverse and longitudinal velocities of sound are calculated from the initial slopes of the corresponding transverse and longitudinal acoustic branches of the dispersion curves in the long wavelength limit. The experimental values of velocities reported in Table 1 are those of longitudinal and transverse sound waves propagating along the c -direction of single crystals of ice at 257 K. It is well known that velocities of sound depend much on the direction of propagation and also on the temperature. Inelastic X-ray scattering data from water at 5 °C shows a variation of the sound velocity from 2000 to 3200 m/s in the momentum range of 1-4 nm⁻¹. The so-called transition from *normal* to *fast* sound in liquid water at ≈ 4 meV, the energy of sound excitations which is equal to the observed second weakly dispersed mode, was reported to be due to the reminiscent of a phonon branch of ice Ih of known optical character (Sette, Ruocco, Krisch, Masciovecchio *et al.*, 1996). We can conclude that our calculated values of longitudinal velocity, v_L is in a reasonable range of velocity of sound in ice along the [100]-direction chosen for our calculation. We must also stress the fact that our phonon dispersions were calculated at 0 K.

4.2 Vibrational density of states of crystalline ice

In order to understand the mode of collective vibration of molecules of water in ice from a spectroscopic point of view, we need to consider the three normal modes of an isolated water molecule shown in Fig. 12 as phases of water vapour; liquid water and ice consist of distinct H₂O molecules recognized by Bernal and Fowler in 1933, which explained one of the factors leading to the Pauli model of the crystal structure of ice. The fact that the forces between the molecules are weak in comparison with the internal bonding results in a simple division of the lattice modes into three groups involving the internal vibrations, rotations, and translations of the molecules. The frequency of the first two groups depend primarily on the mass of the hydrogen or deuterium nuclei, and the frequencies of the translations depend on the mass of the whole molecule (Petrenko and Whitworth, 1999). A free H₂O molecule has just three normal modes of vibration illustrated in Fig. 12. The comparatively small motions of the oxygen atoms are required to keep the centre of mass stationary, and these motions result in the frequency ν_3 being slightly higher than ν_1 ; these depend on the force constant for stretching the covalent O-H bond, while the bending mode ν_2 depends on the force constant for changing the bond angle. In the vapour the free molecules have a rich rotation-vibration infrared spec-

trum (Benedict, Gailar and Plyler, 1956), from which the frequencies of the molecular modes are deduced to be:

$$\begin{aligned}\nu_1 &= 3656.65 \text{ cm}^{-1} \equiv 453.4 \text{ meV}, \\ \nu_2 &= 1594.59 \text{ cm}^{-1} \equiv 197.7 \text{ meV}, \\ \nu_3 &= 3755.79 \text{ cm}^{-1} \equiv 465.7 \text{ meV}.\end{aligned}$$

For ice the band around 400 meV is thus ratified with the O-H bond stretching modes ν_1 and ν_3 . The frequencies are thus lowered from those of the free molecules by the hydrogen bonding to the neighbouring molecules, but as a single molecule cannot vibrate independently, this coupling also leads to complex mode structures involving many molecules.

We can now discuss the vibrational density of states, VDOS, for H₂O ice based on the lattice dynamics obtained from the results of our calculation and compare them to some of the well known spectra of ice such as infrared and Rahman spectra and inelastic neutron scattering data. The total VDOS calculated from the phonon dispersions for our ice structure is shown in Fig. 13. Also shown in Fig. 15 is the corresponding partial VDOS for both hydrogen and the oxygen atoms in the ice system. We note that these phonon DOS are not complete since the summation is not done over the whole Brillouin zone, but only in the [100] direction of the cubic symmetry. The distribution of the partial DOS is given by

$$g_{\alpha,k}(\omega) = \frac{1}{nd\Delta\omega} \sum_{\mathbf{k},j} |e_{\alpha}(k; \mathbf{k}, j)|^2 \delta_{\Delta\omega}(\omega - \omega(\mathbf{k}, j)), \quad (3)$$

where $e_{\alpha}(k; \mathbf{k}, j)$ is the α -th Cartesian component of the polarization vector for the k -th atom; n is the number of sampling points and d is the dimension of the dynamical matrix (Parlinskin, 2002). The total VDOS is calculated by summing all the partial contributions. Figure 13 shows the total VDOS together with the full phonon dispersion curves along the [100] direction. Also shown in Fig. 14 is the enlargement of the intermolecular frequency range on which we superimpose the inelastic neutron-scattering spectra data extracted from Ref. (Cote, Morrison, Cui, Jenkins *et al.*, 2003). The comparison is made with the ice Ih data though our ice structure is not perfectly hexagonal but still there is very little difference between the neutron data for ice Ih and ice geometry used in our calculation in the translational region as explained below. There are well defined separated peaks in the whole range of the vibrations. The illustrative discussion in Fig. 12 can be well understood if we consider the partial DOS in Fig. 15. The covalently O-H stretching mode of both phase and anti-phase, analogous to the frequencies ν_1 and ν_3 for isolated free water molecules, can be seen clearly in Fig. 15(b) in the energy range (350-410 meV) or frequency range (3010-3400 cm⁻¹). We can notice that the collective motion of oxygen is almost static when compared to the collective contributions from the hydrogen atoms. According to

the Rahman spectra, a strong peak is observed at 382.3 meV (3083 cm^{-1} at 95 K) (Bertie and Whalley, 1967; Whalley and Bertie, 1967) for D_2O . If we take into account the mass difference between deuterium and hydrogen atoms (i.e., isotope effect), the peaks which are observed at 2950, 3000 (very short), 3250, and 3270 cm^{-1} are in good range when compared to the experimentally observed values for ν_1 and ν_3 . In the intra-molecular bending region, analogous to the frequency ν_2 for an isolated water molecule ($1580\text{-}1680\text{ cm}^{-1}$), there is an interesting feature. Our results show that, of all the contributions resulting from the collective motion of hydrogen atoms as contribution from collective motion of oxygen atoms is recessive, only *one* of the components of the collective motions of hydrogen atoms contributes to the intra-molecular bending modes and it is one that is dominant. Figure 15(b) gives an example of such contribution being dominated mainly by the y -component of the intra-molecular vibration of the O-H. This means that intra-molecular bending of the angular motion takes place mostly in one direction.

Tanaka has identified hydrogen-bond bending modes with negative expansion coefficients associated with this region (Tanaka, 1998). If we go further down to the low frequency region such as $600\text{-}1200\text{ cm}^{-1}$ called the molecular librational region and then to ($0\text{-}400\text{ cm}^{-1}$) called the molecular translational region, where we estimated the sound velocities from the corresponding phonon dispersion curve, the VDOS peaks of these modes of vibration agree very well with the experimental observation from inelastic neutron scattering data. The general agreement of the features in the translational optic region is good with all the three distinct peaks present at 400, 270 and 105 cm^{-1} (Li, 1996).

4.3 The boson peak in ice

The high frequency ($0.1\text{-}10\text{ THz}$) or energy ($0.4136\text{-}41.36\text{ meV}$) excitations have been experimentally shown to have linear dispersion relations in the mesoscopic momentum region ($\sim 1\text{-}10\text{ nm}^{-1}$). So many amorphous materials display low temperature anomalies in their specific heats that they are generally regarded as being universal properties of the glassy state. These anomalies are usually of two kinds. The first concerns observation that, while many crystals obey the Debye law $C \propto T^3$ for temperatures less than say, 1K, glasses with the same chemistry frequently display the law $C \propto T$ at correspondingly low temperature (Phillips, 1996). This second observation is tied in with the appearance of the ubiquitous Boson peak (BP) in inelastic neutron and Raman spectra (Buchenau, Zhou, Nucker, Gilroy *et al.*, 1987). The name Boson peak therefore refers to the fact that the temperature dependence of its intensity scales roughly with the Bose-Einstein distribution. Dove *et al.* demonstrated that the Boson peak arises largely from a flattening of the dispersion of the transverse acoustic modes, in a manner similar to that which occurs in a crystalline material at its Brillouin zone bound-

ary (Dove, Harris, Hannon, Parker *et al.*, 1997). This idea is not new, being originally suggested by (Leadbetter, 1969), and recently developed further by (Elliott, 1996; Taraskin, 1997; Taraskin and Elliot, 1997). A standard way of extracting the boson peak (BP) from the vibrational spectrum is to plot $g(E)/E^2$ (as done in Fig. 16(b)), since in the Debye approximation $g(E) \approx E^2$ at low energy. In Fig. 16 we show the plot of $g(E)$ and the corresponding $g(E)/E^2$ in the translational low energy range for the ice geometry in our calculation. According to the Debye law, it is expected that $g(E)/E^2$ should be constant for the whole range of energy. This constant relation is only obtained at energies larger than 40 meV in agreement with the experimental observation range for the BP as mentioned above. There is an anomalous sharp peak at 3.5 meV which can be ascribed to the region of low-energy *excess* vibrational excitation of the so-called BP. The reason for this peak is unknown since we have a crystalline structure for our ice geometry. The peak reveals the anomalous behaviour of hydrogen bonding in the crystal ice which shows similarity in the behaviour as in the results of an inelastic neutron scattering study of a crystalline polymorph of SiO_2 (α -quartz), and a number of silicate glasses (pure silica, SiO_2) with tetrahedral coordination (Harris *et al.*, 2000). Also amorphous solids, most supercool liquids and the complex systems show this anomalous character (Grigera, Martin, Parisi and Verrocchio, 2003).

5. SUMMARY

Our MD simulation, carried out through the analysis of radial distribution functions of the ice crystal, shows fair agreement in the positions of peaks in comparison with neutron diffraction data.

The phonon dispersion calculations in [100] direction shows a good result especially in the acoustic region in comparison with experiment. Our optic modes are degenerate at the Γ -point due to application of the direct method used in this calculation which does not take into account the effect of polarization arising from dipole-dipole interactions of water molecules which is expected to yield a significant effect in the splitting of longitudinal and transverse optic modes at the Γ -point. We intend to include this polarization effect in our future work through the calculation of effective charge tensors using the Berry phase approach to see actually if there will be splitting. Our calculated longitudinal acoustic velocity agrees well with the longitudinal acoustic velocity from inelastic neutron scattering data. The vibrational density of states reproduces all the features in covalently O-H stretching region, intra-molecular bending region, molecular librational region as well as in the molecular translational region, when comparing our results to some infrared spectra, Rahman spectra as well as inelastic neutron scattering results.

The analysis of the vibrational density of states shows a boson peak, a characteristic feature common to amorphous systems, at low energy of the translational region. The anomalous sharp peak of $g(E)/E^2$ at 3.5 meV, which

can be ascribed to the region of low-energy *excess* vibrational excitation of the boson peak, might be due to the anomalous behaviour of hydrogen bonding since we have a perfect crystal. The origin of this anomalous behaviour of this abnormal peak in non-crystalline solids and supercool liquids is still subject of scientific debate.

Acknowledgments

We acknowledge the support by the Deutsche Forschungsgemeinschaft (Graduate College “*Structure and Dynamics of Heterogeneous Systems*”).

We thank Prof. Keith Ross for allowing us to use one of their phonon dispersions for comparison with our results. Also, we acknowledge Prof. Soper for providing us the neutron diffraction data of radial distribution functions of liquid water and ice for fitting our *ab-initio* simulation results.

References

- Benedict, W. S., N. Gailar and E. K. Plyler (1956). Rotation-vibration spectra of deuterated water vapour. *J. Chem. Phys.*, **24**, 1139.
- Bernal, J. D. and R. H. Fowler (1933). A theory of water and ionic solution. *J. Chem. Phys.*, **1**, 515.
- Bertie, J. E. and E. Whalley (1967). Optical spectra of orientationally disordered crystals. II. infrared spectrum of ice Ih and ice Ic from 360 to 50 cm^{-1} . *J. Chem. Phys.*, **46**, 1264.
- Blackman, M. and N. D. Lisgarten (1958). Elect diff of cubic & other struc forms of ice. *Adv. Phys.*, **7**, 189.
- Buchenau, U., H. M. Zhou, N. Nucker, K. S. Gilroy *et al.* (1987). Nature of vibrational excitations in vitreous silica. *Phys. Rev. Lett.*, **60**, 1318.
- Cote, A. S., I. Morrison, X. Cui, S. Jenkins *et al.* (2003). Ab-initio density-functional lattice-dynamics studies of ice. *Can. J. Phys.*, **81**, 115.
- Dove, M. T., M. J. Harris, A. C. Hannon, J. M. Parker *et al.* (1997). Floppy modes in crystalline and amorphous silicates. *Phys. Rev. Lett.*, **78**, 1070.
- Elliott, S. R. (1996). Comment on ”phonons in glasses: Numerical simulations and phenomenological theory”. *Phys. Rev. Lett.*, **77**, 4105.
- Faure, P. P. (1969). Étude d’un modèle dynamique du réseau cristallin de la glace. *J. Physique (France)*, **30**, 214.
- Gammon, P. H., H. Kiefte, M. J. Clouter and W. W. Denner (1983). Elastic constants of artificial and natural ice samples by Brillouin spectroscopy. *J. Glaciology*, **29**(103), 433.

- Grigera, T. S., V. Martin, G. Parisi and P. Verrocchio (2003). Phonon interpretation of the 'boson peak' in supercooled liquids. *Nature*, **422**, 289.
- Harris, M. J., M. T. Dove and J. M. Parker (2000). Floppy modes and boson peak in crystalline and amorphous silicates: an inelastic neutron scattering study. *Mineralogical Magazine*, **64**, 435.
- Klug, D. D. and E. Whalley (1978). Origin of the high-frequency translational bands of ice I. *J. Glaciology*, **21**, 55.
- Kresse, G. and J. Futhmüller (1996). Efficient iterative schemes for ab initio total-energy calculations using a plane-wave basis set. *Phys. Rev. B*, **54**, 11169.
- Leadbetter, A. J. (1969). Inelastic cold neutron scattering from different forms of silica. *J. Chem. Phys.*, **51**, 779.
- Lee, C., D. Vanderbilt, K. Laarsonen, R. Car *et al.* (1993). Ab-initio studies on the structural and dynamical properties of ice. *Phys. Rev. B*, **47**, 4863.
- Li, J. (1996). Inelastic neutron scattering studies of hydrogen bonding in ices. *J. Chem. Phys.*, **105**, 6733.
- Marchi, M., J. S. Tse and M. Klein (1986). Lattice vibrations and infrared absorption on ice Ih. *J. Chem. Phys.*, **85**, 2414.
- Morrison, I. and S. Jenkins (1999). First-principles lattice dynamics studies of the vibrational spectra of ice. *Physica B*, **263**, 442.
- Nielsen, G., R. M. Townsend and S. A. Rice (1984). Model based calculations of the lattice mode spectra of ice Ih and amorphous solid water. *J. Chem. Phys.*, **81**, 5288.
- Nielson, G., R. M. Townsend and S. A. Rice (1984). Model based calculations of the lattice mode spectra of ice Ih and amorphous solid water. *J. Chem. Phys.*, **81**, 5288.
- Parlinskin, K. (2002). *Phonon*. Cracow, Poland, Software, Version 3.11.
- Parlinskin, K., Z. Q. Li and Y. Kawazoe (1997). First-principles determination of the soft mode in cubic ZrO_2 . *Phys. Rev. Lett.*, **78**, 4063.
- Pauling, L. (1935). The structure and entropy of ice and of other crystals with some randomness of atomic arrangement. *J. Am. Chem. Soc.*, **57**, 2680.
- Petrenko, V. F. and R. W. Whitworth (1999). *Physics of Ice*. Oxford University Press, Oxford.
- Phillips, W. A. (1996). Two-level states in glasses. *Rep. Prog. Phys*, **50**, 1657.
- Prask, H. J. and S. F. Trevino (1972). Ice I-lattice dynamics and incoherent neutron scattering. *J. Chem. Phys.*, **56**, 3217.

- Renker, B. (1973). *Physics and Chemistry of Ice*. (University of Toronto Press), p. 82, Toronto.
- Renker, B. and P. V. Blanckenhagen (1969). *Physics of Ice*. Plenum, New York.
- Sette, F., G. Ruocco, M. Krisch, C. Masciovecchio *et al.* (1996). Transition from normal to fast sound in liquid water. *Phys. Rev. Lett.*, **77**, 83.
- Soper, A. K. (2000). The radial distribution functions of water and ice from 220 to 673 K and at pressure up to 400 MPa. *Chem. Phys. Lett.*, **258**, 121.
- Srivastava, G. P. (1990). *The Physics of Phonons*. Adam Hilger, New York.
- Svishchev, I. M. and P. G. Kusalik (1994). Crystallization of liquid water in a molecular dynamics simulation. *Phys. Rev. Lett.*, **73**, 975.
- Tanaka, H. (1998). Thermodynamic stability and negative thermal expansion of hexagonal and cubic ices. *J. Chem. Phys.*, **108**, 4887.
- Taraskin, S. N. (1997). Phonons in vitreous silica: Dispersion and localization. *Europhys. Lett.*, **39**, 37.
- Taraskin, S. N. and S. R. Elliot (1997). Nature of vibrational excitations in vitreous silica. *Phys. Rev. B*, **56**, 8605.
- Tse, J. S., M. L. Klein and I. R. McDonald (1984). Lattice vibrations of ices Ih, VIII, and IX. *J. Chem. Phys.*, **81**, 6124.
- Whalley, E. and J. E. Bertie (1967). Optical spectra of orientationally disordered crystals. I. theory of translational lattice vibrations. *J. Chem. Phys.*, **46**, 1264.
- Xantheas, S. S. and H. T. Dunning (1993). *Ab initio* studies of cyclic water clusters $(\text{H}_2\text{O})_n$, $n = 1-6$. I. Optimal structures and vibrational spectra. *J. Chem. Phys.*, **99**, 8774.
- Zayak, A. T., P. Entel, J. Enkovaara, A. Ayuela *et al.* (2003). A first-principles investigation of phonon softenings and lattice instabilities in the shape memory system Ni_2MnGa . *Phys. Rev. B*, **68**, 132402.

TABLES

Table 1 Velocities of sound calculated from the initial slope of the phonon dispersion curves of ice in $[100]$ direction compared to the experimental result.

FIGURE CAPTIONS

- Fig. 1** The phase diagram of the stable phases of ice.
- Fig. 2** The tetrahedral unit from which the hexagonal ice is created.
- Fig. 3** Initial and the relaxed geometry of the unit cell of ice. The ice structure was initially packed in a cubic unit cell with initial lattice constant taken from the literature (Lee, Vanderbilt, Laarsonen, Car *et al.*, 1993) to be 6.35 Å. There are no hydrogen bonds in the initial prepared structure shown on the left but were perfectly formed after the relaxation. The relaxed geometry has the values of $a \approx b \neq c$ which implies that the relaxed structure is tetragonal with c/a ratio ≈ 0.988 .
- Fig. 4** Relaxed crystalline structure of ice produced from the geometry in Fig. 2 by replicating in all direction by the calculated lattice parameters.
- Fig. 5** Distribution of H-O-H angle in ice and water (in arbitrary units). The comparison is done for the ice at 220 K and liquid water simulated at room temperature (298 K) and at high temperature in the supercritical regime. The H-O-H angles of ice structure are larger compared to those of liquid water.
- Fig. 6** Radial distribution functions g_{OO} and g_{OH} at 100 K and 220 K obtained with VASP. There is a gradual loss of long-range order at 220 K as can be noticed in its 2nd and 3rd peaks of g_{OO} when compared to the results for 100 K.
- Fig. 7** Radial distribution functions g_{HH} at 100 K and 200 K obtained with VASP. There is a gradual “loss of peaks” observed for temperature 100 K at 2.5, 4.4, 4.8 and 5.4 Å due to the loss of long-range order as the temperature increases.
- Fig. 8** Radial distribution functions g_{OO} and g_{OH} at 220 K obtained with VASP compared to neutron diffraction scattering data (NDS) (Soper, 2000).
- Fig. 9** Radial distribution functions g_{HH} obtained with VASP at 220 K compared to neutron diffraction scattering data (NDS) (Soper, 2000).
- Fig. 10** (I) Brillouin zone for the cubic symmetry used in our VASP calculation of the ice system. Our phonon dispersions are calculated in [100] k_x -direction, (II) The first Brillouin zone for the structure of ice Ih with origin at the point Γ . $\Gamma A = \frac{1}{2}c^*$ and $\Gamma M = \frac{1}{2}a^*$, where a^* and c^* are the vectors of the reciprocal lattice

(Petrenko and Whitworth, 1999). The dispersion curves are commonly drawn along the lines of symmetry ΓA , ΓM , and ΓK .

- Fig. 11** (a) With VASP calculated phonon dispersion curves of ice in [100] direction of the tetragonal unit cell compared to (b) dispersion relations in the translational frequency range for the ice structure plotted along the Cartesian directions from zone center to zone edge in the Brillouin zone of the orthorhombic eight-molecule unit cell (Cote *et al.* (Cote, Morrison, Cui, Jenkins *et al.*, 2003)) and (c) the experimental dispersion of D₂O ice according to Renker's model (Renker, 1973). The difference in scale of (c) from (a) and (b) is due to the isotopic effect because of difference in the masses of hydrogen and Deuterium atoms.
- Fig. 12** The three normal modes of an isolated water molecule. Motion with frequency ν_1 can be regarded as symmetric stretch, ν_2 as bending and ν_3 as anti-symmetric (Petrenko and Whitworth, 1999).
- Fig. 13** Total vibrational density of states (VDOS) of ice based on the lattice dynamics together with full phonon dispersion curves. The VDOS show all the important regions such as the intermolecular translational, librational, bending and the stretching frequency range.
- Fig. 14** Enlargement of calculated total vibrational density of states in Fig. 13 showing the intermolecular range of frequencies. The broken line is taken from the inelastic neutron scattering data available through Ref. (Cote, Morrison, Cui, Jenkins *et al.*, 2003).
- Fig. 15** Partial density of states of ice based on the lattice dynamics. (a) shows the x , y and z components of VDOS for the oxygen atoms in the H₂O ice. (b) shows the x , y and z VDOS for corresponding hydrogen atoms for the whole range of frequencies. It is interesting to notice that in the intra molecular bending region (1580-1680 cm⁻¹), only one of the components of the VDOS of hydrogen (say y) dominates while x and z contribute less. The contribution from the oxygen atoms can be regarded as being completely recessive in this region.
- Fig. 16** Plot of the VDOS $g(E)$ and the corresponding $g(E)/E^2$ vs. E for the region of translational mode. The boson peak is found in the low-energy region at 3.5 meV.

Table 1: W. A. Adeagbo et. al.

$\times 10^3$ m/s	Experiment ^a	Theory
v_{LA}	4.04	4.86
v_{TA}	1.80	3.02

^a (Gammon, Kiefte, Clouter and Denner, 1983)

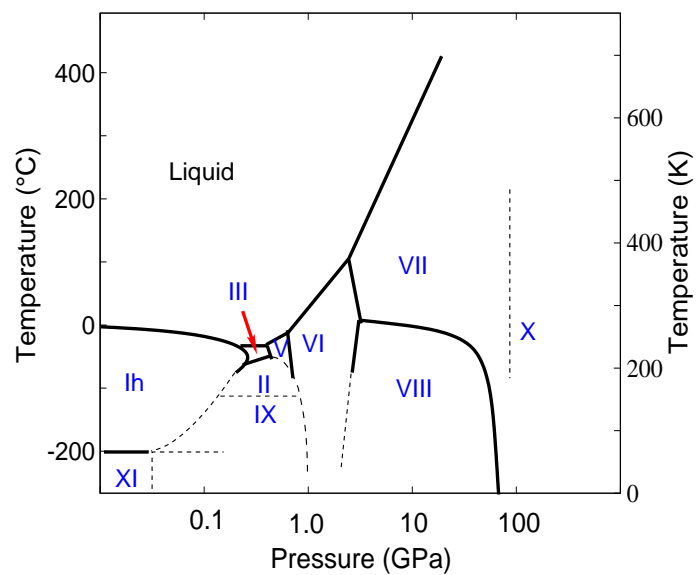


Figure 1: W. A. Adeagbo et. al.

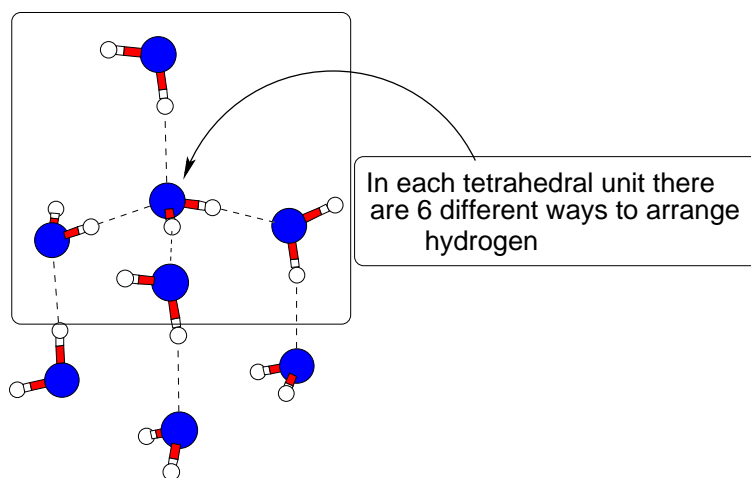


Figure 2: W. A. Adeagbo et. al.

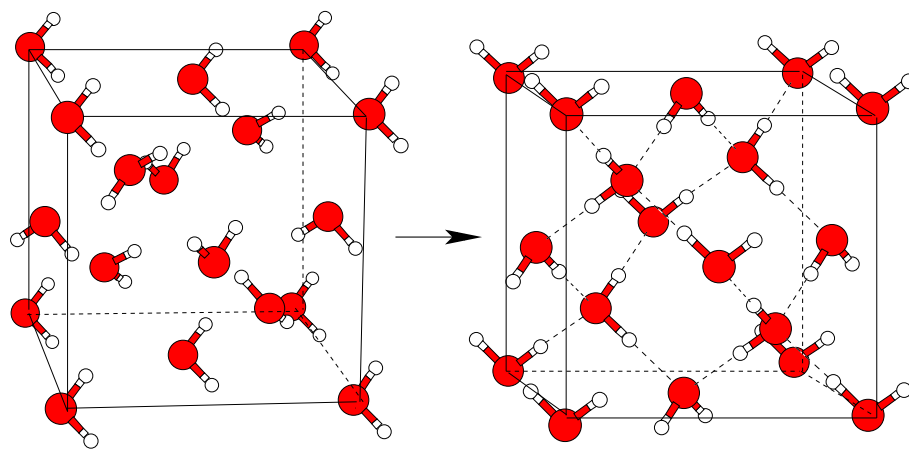


Figure 3: W. A. Adeagbo et. al.

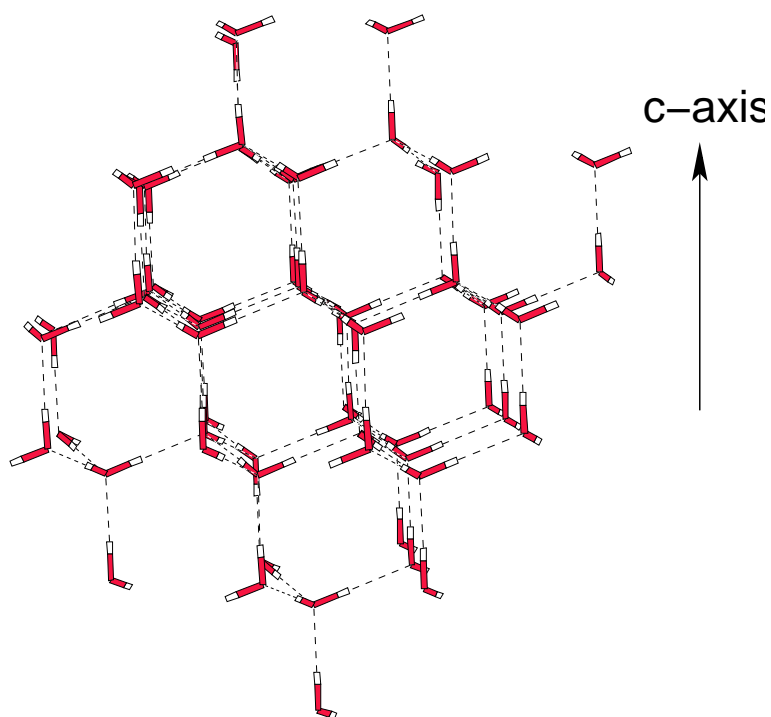


Figure 4: W. A. Adeagbo et. al.

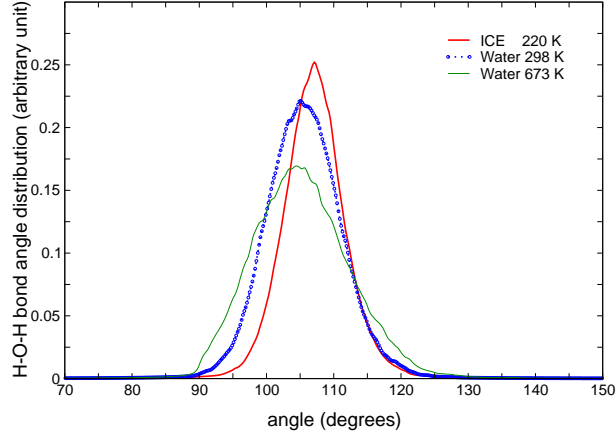


Figure 5: W. A. Adeagbo et. al.

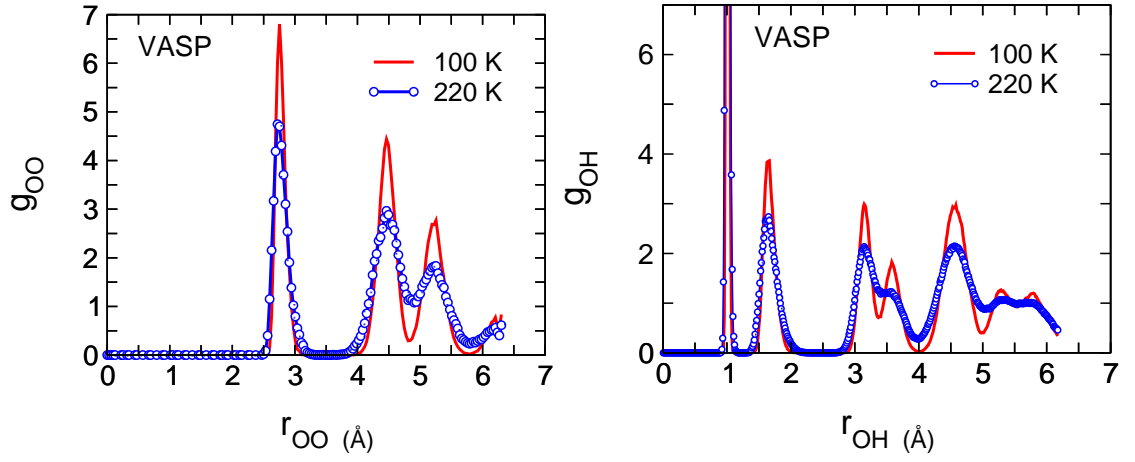


Figure 6: W. A. Adeagbo et. al.

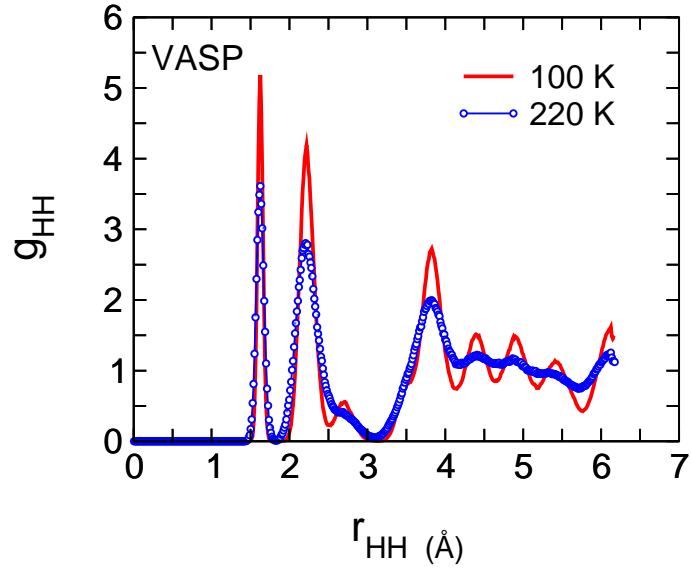


Figure 7: W. A. Adeagbo et. al.

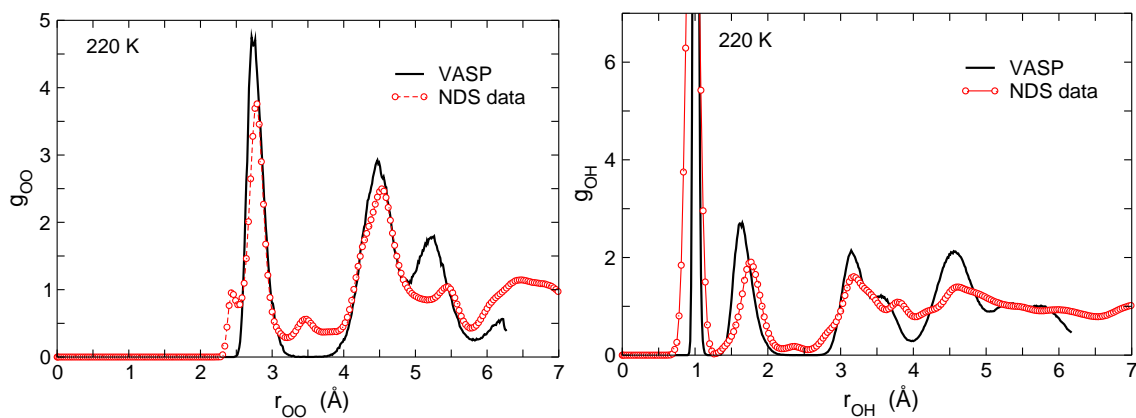


Figure 8: W. A. Adeagbo et. al.

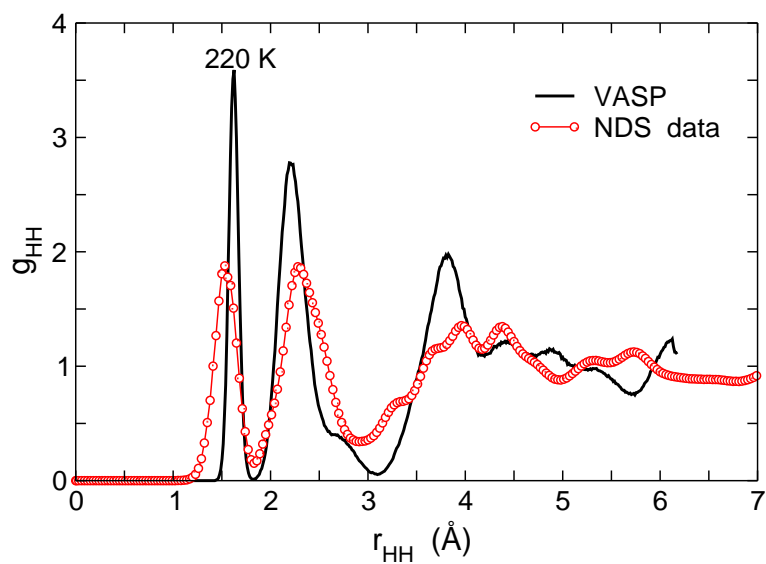


Figure 9: W. A. Adeagbo et. al.

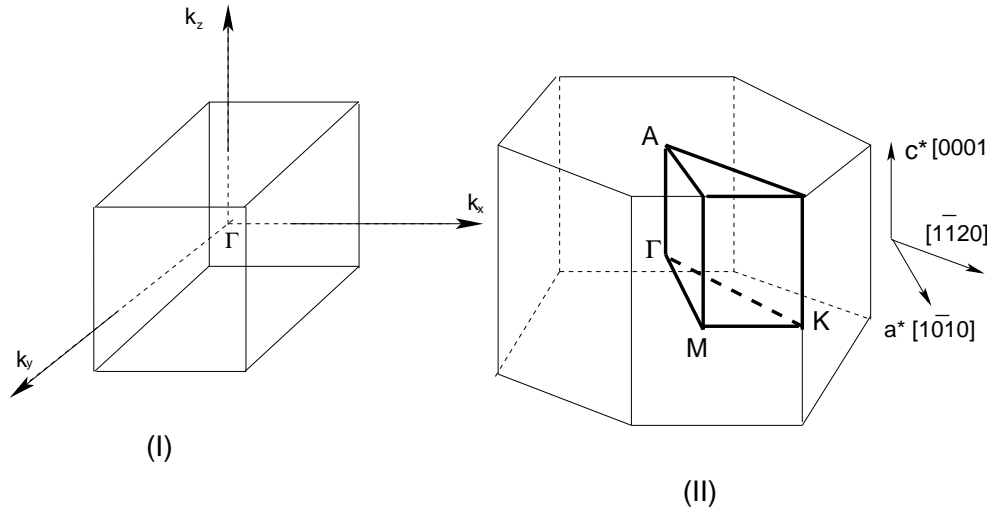


Figure 10: W. A. Adeagbo et. al.

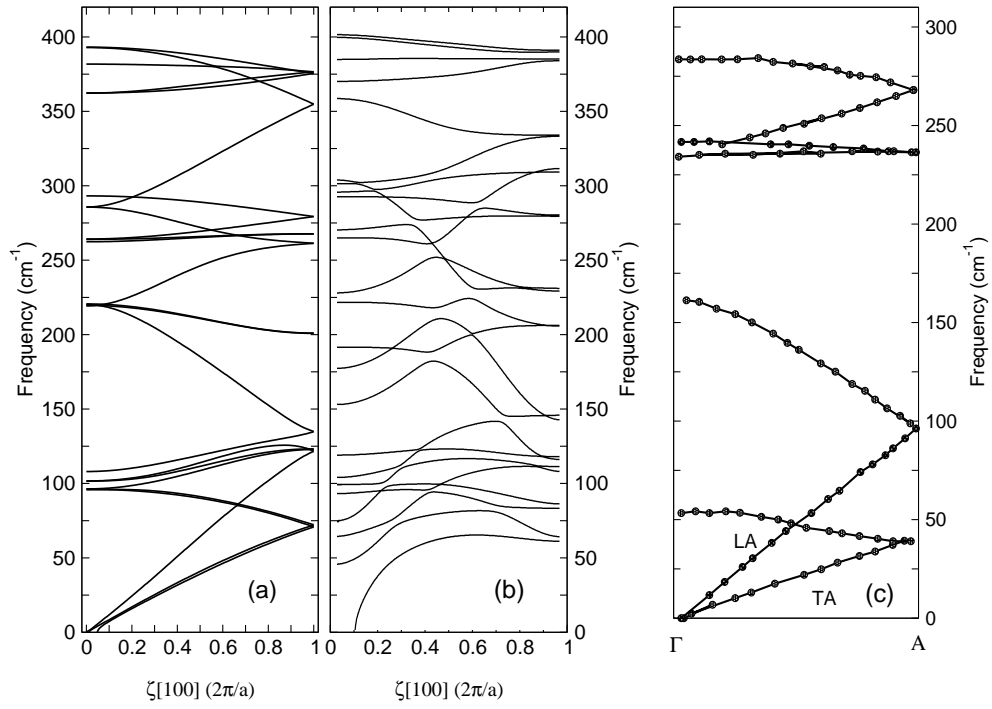


Figure 11: W. A. Adeagbo et. al

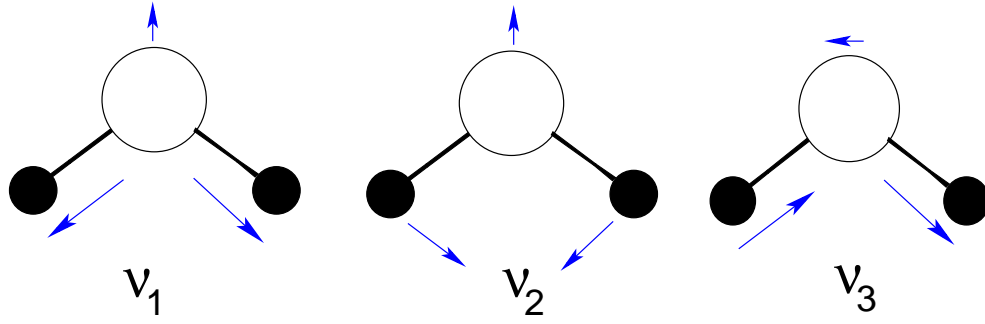


Figure 12: W. A. Adeagbo et. al.

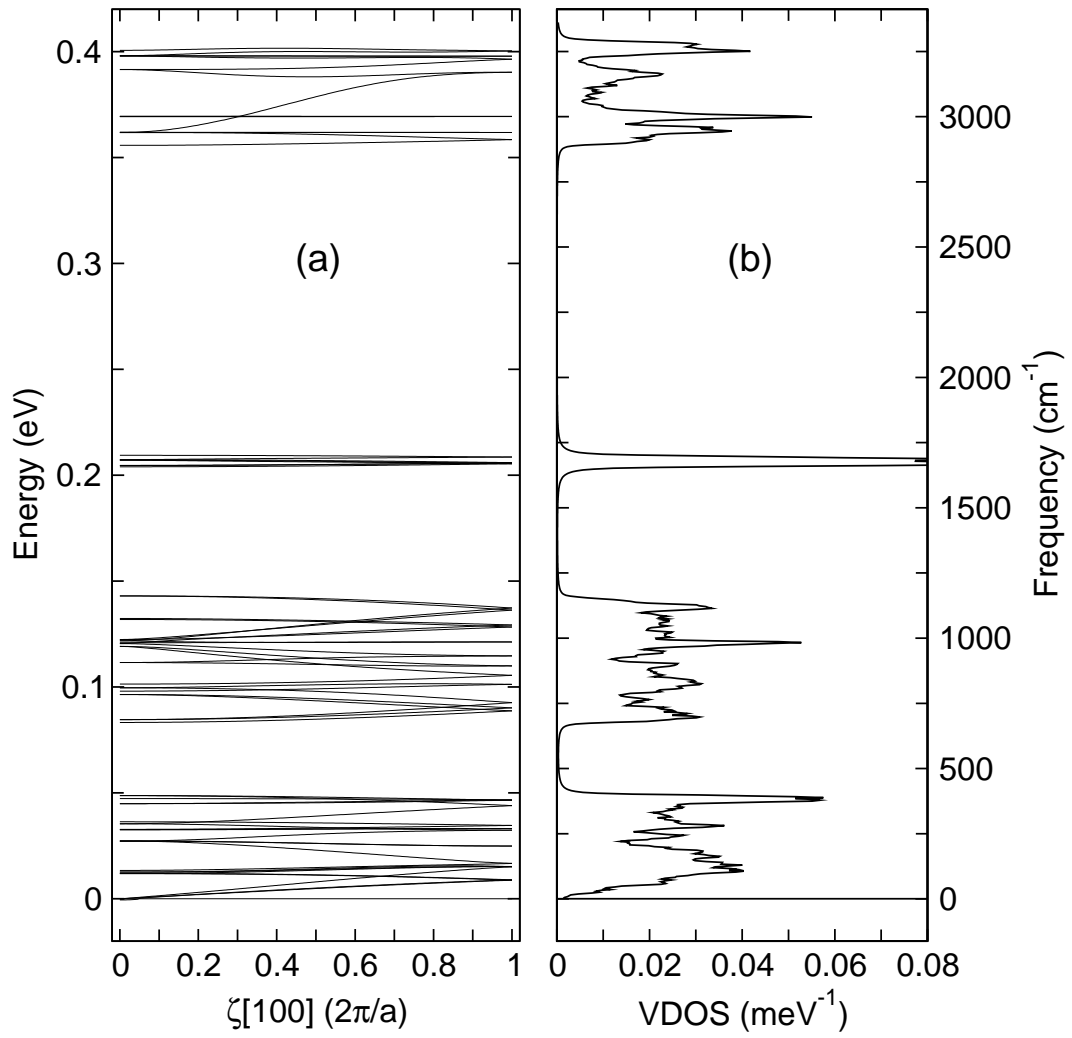


Figure 13: W. A. Adeagbo et. al.

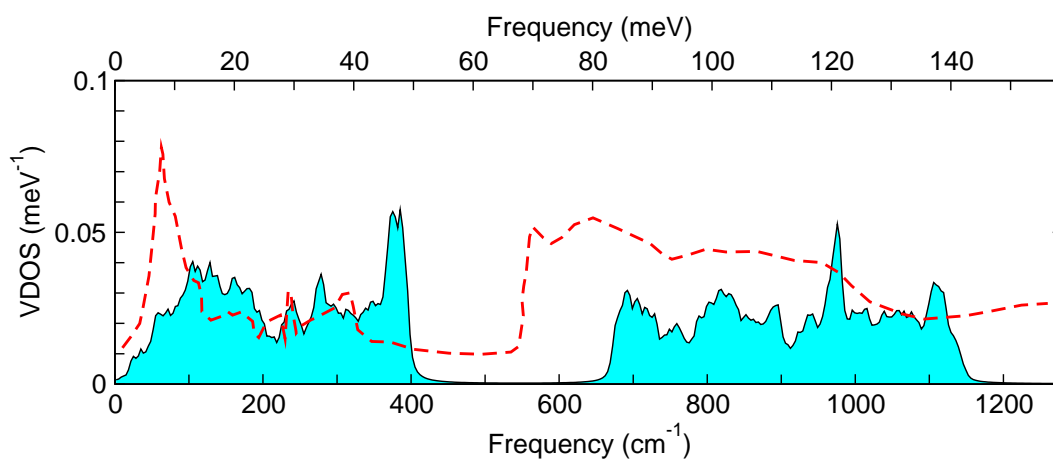


Figure 14: W. A. Adeagbo et. al.

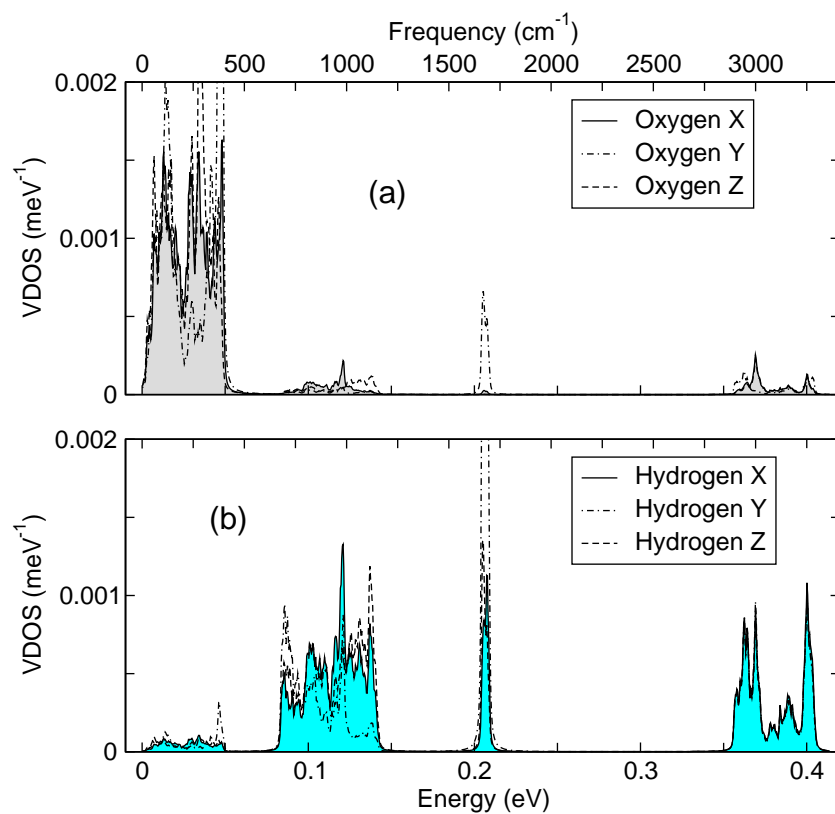


Figure 15: W. A. Adeagbo et. al.

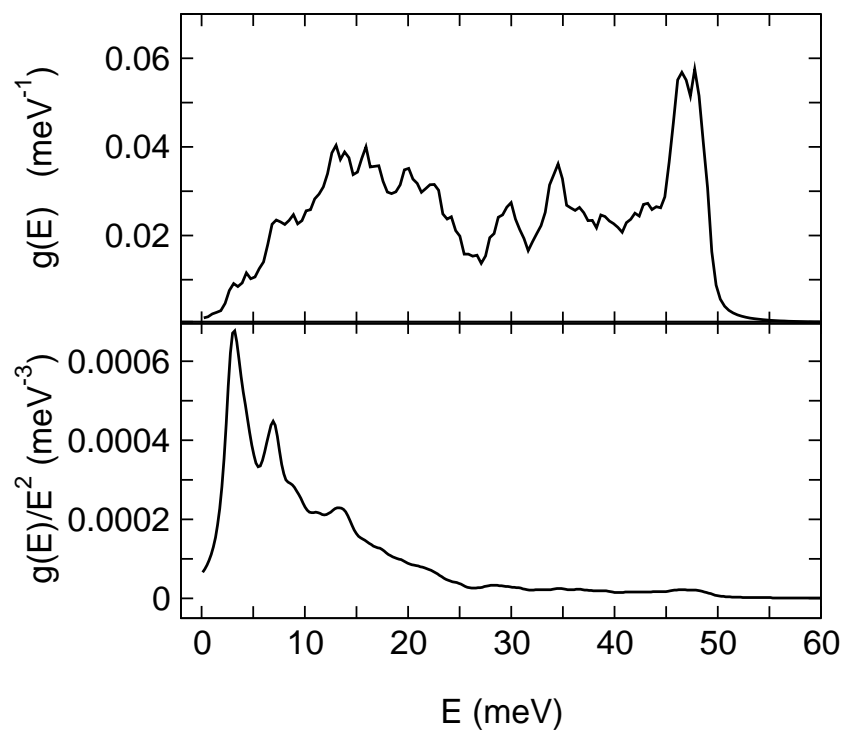


Figure 16: W. A. Adeagbo et. al.